

1 **The Andes Affect ENSO Statistics**

2 Weixuan Xu,^a Jung-Eun Lee,^a Baylor Fox-Kemper,^a Yann Planon,^b and Michael J. McPhaden^b

3 ^a *Department of Earth, Environmental and Planetary Sciences, Brown University, Providence,*
4 *Rhode Island, U.S.A.*

5 ^b *Pacific Marine Environmental Laboratory, NOAA/PMEL, Seattle, Washington, U.S.A.*

6 *Corresponding author:* weixuan_xu@brown.edu

7 ABSTRACT: Current coupled global climate models have biases in their simulations of the tropical
8 Pacific mean state conditions as well as the El Niño Southern Oscillation (ENSO) phenomenon.
9 Specifically, in the Community Earth System Model (CESM version 1.2.2), the tropical Pacific
10 mean state has overly weak sea surface temperature (SST) gradients in both the zonal and meridional
11 directions, ENSO is too strong and too regular, and El Niño and La Niña events are too symmetrical.
12 A previous study with a slab ocean model showed that a higher elevation of the Andes can improve
13 the tropical Pacific mean state simulation by adjusting the atmospheric circulation and increasing
14 the east-west and north-south SST gradients. Motivated by the link between the mean tropical
15 Pacific climate and ENSO variations shown in previous studies, here we explored the influence of
16 the Andes on the simulation of ENSO using the CESM 1.2.2 under full atmosphere-ocean coupling.
17 In addition to improving the simulated tropical Pacific mean state by increasing the strength of
18 the surface easterly and cross-equatorial southerly winds, the Higher Andes experiment decreases
19 the amplitude of ENSO, increases the phase asymmetry, and makes ENSO events less regular,
20 resulting in a simulated ENSO that is more consistent with observations. The weaker ENSO cycle
21 is related to stronger damping in the Higher Andes experiment according to an analysis of the
22 Bjerknes Index. Our overall results suggest that increasing the height of the Andes reduces biases
23 in the mean state and improves the representation of ENSO in the tropical Pacific.

24 **1. Introduction**

25 The tropical Pacific climate is formed by the large-scale interaction between the atmosphere and
26 the ocean. Its mean state has strong contrast between the wet and warm western Pacific and the cold
27 and dry eastern Pacific. Deviating from this mean state, the tropical Pacific climate has a natural
28 interannual variation called El Niño/Southern Oscillation (ENSO, see McPhaden et al. (2020) for a
29 review). ENSO events alter the global atmospheric circulation, causing unusual floods or droughts
30 occur in many regions (e.g., Prieto 2007), creating threats to our society in many aspects including
31 agriculture (Nicholls 1991), fisheries (Lehodey et al. 2020), public safety (Fang et al. 2021), and
32 economic vitality (Bastianin et al. 2018).

33 Due to ENSO's impacts, understanding its dynamics and predicting it a few seasons in advance
34 has been the focus of intensive research over the last 50 years. Early methods built simplified
35 models to simulate the components that affect ENSO's initiation, generation and dissipation (e.g.
36 Bjerknes 1969; Wyrski 1985; Cane and Zebiak 1985; Jin 1996, 1997a,b). These simplified climate
37 models do simulate a quasi-periodic signal and reveal some of the key components of the ENSO
38 cycle, but many important aspects of ENSO are not accounted for. With the lack of seasonal
39 modulation and the non-linear processes in these simplified models, they are too limited in scope
40 and cannot reproduce the full complexity and diversity of ENSO (Jin et al. 2020; Levine et al. 2016).
41 Coupled Global Circulation Models (CGCMs) are better suited to capture many characteristics of
42 ENSO compared with simplified models, but they still have a lot of systematic errors (Guilyardi
43 et al. 2009; Bellenger et al. 2014; Guilyardi et al. 2020; Planton et al. 2021), including biases
44 in the mean state, in processes contributing to the growth and decay of ENSO and occurrence
45 statistics. Biases in the mean state include the SST distribution, double Inter-Tropical Convergence
46 Zones (ITCZs) bias, and the errors in surface wind simulation (e.g., Guilyardi et al. 2020; Planton
47 et al. 2021). Biases in ENSO properties include the wrong amplitude, too sharply peaked power
48 spectrum, excess westward displacement of the ENSO pattern, too little skewness and so on (e.g.,
49 Guilyardi et al. 2020; Planton et al. 2021). In addition, there are still considerable uncertainties in
50 ENSO properties under warmer climate, although climate models are improving in the agreement
51 of future projections (Cai et al. 2018, 2021).

52 Progress in overcoming these difficulties has taken many forms. One solution is increasing the
53 spatial and temporal resolutions of the atmosphere and ocean models (Wittenberg et al. 2018).

54 However, it is a slow and challenging process to reach higher resolution model simulations, since
55 each increase in resolution is exponentially more difficult. Fox-Kemper et al. (2014) showed that the
56 past decades' rate of computational improvement results in the doubling of full-complexity CGCM
57 resolution only every 10.2 years (consistent with a recent update by Haine et al. 2021). Therefore,
58 instead of using a higher-resolution climate model, we attempt to improve ENSO simulations by
59 better representing dynamical processes.

60 As many errors in ENSO properties and errors in the mean state climate are closely connected
61 (e.g., Zhang and Sun 2014; Abellán et al. 2017; He et al. 2018), adjustments that can improve
62 the mean state simulations may also improve the ENSO simulation. The mean state over the
63 Pacific can be influenced by many aspects of the modeling system, but the focus in this paper
64 is the representation of the Andes. Previous studies showed that removing all orography in a
65 CGCM modulates the mean states and ENSO has a stronger amplitude and increased regularity
66 (Kitoh 2007; Naiman et al. 2017). As the Andes alone are important for the formation of the
67 southeast Pacific cold tongue (Takahashi and Battisti 2007), Xu and Lee (2021) hypothesized that
68 the Andes are not high enough in the low-resolution CGCMs and improving that could improve the
69 simulation of the Pacific mean state and variability. Indeed, with too low Andes, the modeled range
70 insufficiently modulates the atmospheric circulation and result in too warm SST in the southeast
71 Pacific and too much precipitation over the south Pacific. To test this hypothesis, Xu and Lee (2021)
72 modified the Andes in a coupled system with a slab-ocean model and compared the experiment
73 with a higher elevation of the Andes model versus a control experiment with the standard coarsened
74 Andes orography. They found an improvement in the simulation of the tropical Pacific mean state
75 with lowered SST in the southeast Pacific cold tongue and the inhibition of precipitation over the
76 central south Pacific. We hypothesize that modifying the Andes will affect ENSO as well.

77 In this paper, we explore whether modification of the Andes can improve simulations of the
78 mean state climate and the ENSO cycle in the tropical Pacific using a CGCM, focusing on the role
79 of upper ocean dynamical feedbacks. Section 2 introduces the experimental setup and the model
80 setting. Section 3 and 4 compare the model results in terms of the mean state and ENSO cycle.
81 Section 5 discusses the mechanism explanations of our result and Section 6 talks about its scientific
82 importance.

83 2. Method

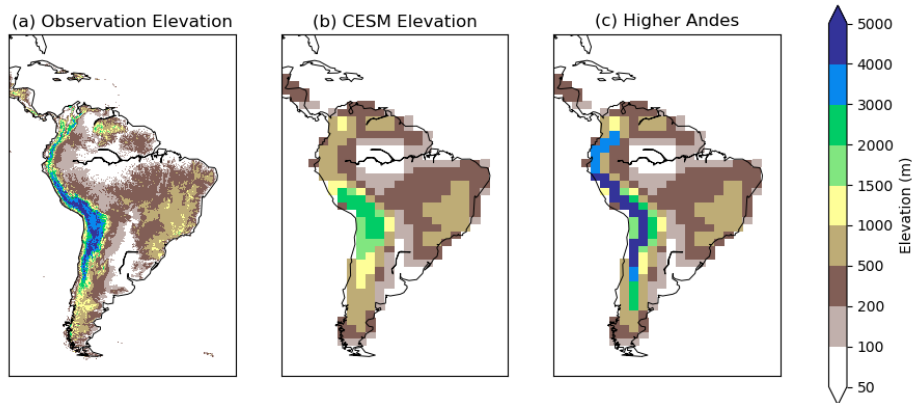
84 *a. Model and Experiment*

85 We used the National Center for Atmospheric Research (NCAR) Community Earth System
86 Model (CESM) version 1.2.2 (Hurrell et al. 2013). It includes the Community Atmospheric
87 Model, version 4 (CAM4) as the atmosphere component, and an extension of the Parallel Ocean
88 Program (POP) Version 2 from Los Alamos National Laboratory (LANL) as the ocean component.
89 We ran the model with CO₂ concentration as in year 2000 (367 ppm) so that we can compare our
90 result with the satellite data. We used the atmospheric resolution of $1.9^\circ \times 2.5^\circ$ with 26 vertical
91 layers and nominal oceanic resolution of 1° with 60 vertical layers for our experiment.

92 Boos and Kuang (2010) showed that the narrow Himalayas mountain ranges, rather than the
93 Tibetan plateau, is essential to modulate the South Asian monsoon. Inspired by their study, we
94 consider the Andes as a similar barrier that influences the tropical Pacific circulations. Fig. 1a
95 shows the 1-km high-resolution topography from the National Oceanic and Atmospheric Adminis-
96 tration (NOAA) National Geophysical Data Center (NGDC) Global Land One-km Base Elevation
97 (GLOBE) topography, and Fig 1b is the default topography setting in CESM (used in our control
98 experiment). In order to understand the influence from the Andes, we modified the height of
99 the Andes to the highest value according to the GLOBE topography (Fig. 1c; experiment called
100 'Higher Andes'). In each coarse-grained grid cell along the Andes in the climate model, we com-
101 puted its elevation as the maximal elevation within the cell area of the fine-grained observations.
102 Our approach is to evaluate the maximum possible influence of the Andes, and not to simulate the
103 exact influence of the Andes. Both experiments were run for 350 years to allow the upper ocean to
104 adjust to the modification, and we used the last 160 years of model output for our analysis.

111 *b. Analysis*

112 To analyze the model performance, we used the ENSO metrics package developed by the
113 International Climate and Ocean: Variability, Predictability and Change (CLIVAR) Pacific Region
114 Panel (Planton et al. 2021). These metrics allow us to rapidly diagnose and evaluate the model's
115 performance regarding the ENSO-related mean state and properties, teleconnection pattern, and
116 dynamical coupling. In this research, we will focus on the comparison of the simulation accuracy
117 between the Control and Higher Andes experiments.



105 FIG. 1. Elevation in South America from (a) National Oceanic and Atmospheric Administration (NOAA)
 106 National Geophysical Data Center (NGDC) Global Land One-km Base Elevation (GLOBE) topography, (b) 1.9°
 107 $\times 2.5^\circ$ resolution of CESM Control experiment topography, and (c) Higher Andes experiment topography. The
 108 height of the Andes is adjusted to the highest value according to the GLOBE topography: in each coarse-grained
 109 grid cell along the Andes in the climate model, we computed its elevation as the maximal elevation within the
 110 cell area of the fine-grained observations. Same as Fig. 1 in Xu and Lee (2021).

118 To evaluate the model's performance on the tropical Pacific climate, we use HadISST's SST
 119 (Rayner et al. 2003), GPCPv2.3's precipitation (Adler et al. 2003), TropFlux's net surface heat
 120 fluxes and surface wind stress (Praveen Kumar et al. 2012, 2013), and the Met Office Hadley
 121 Centre's EN4 ocean temperature profile (Good et al. 2013). We use monthly data from these
 122 products over the period 1979 to 2018. Although the CO_2 forcing within this period is not constant
 123 as in the model, it increases linearly with the average value approximately equal to that in year
 124 2000. Therefore we still consider it a fair comparison.

125 To compare the spatial distributions between the observations and the simulations, all data is
 126 interpolated onto a regular $1^\circ \times 1^\circ$ grid. The gridded observational datasets available are not
 127 perfect and choosing another group of datasets may slightly change the metric values (e.g., Planton
 128 et al. 2021). Using these observational datasets we do not precisely evaluate the model, but merely
 129 detect the differences between the Control and Higher Andes experiments and estimate if the new
 130 simulation is getting better or worse.

131 In the evaluation of the mean state distribution (Fig. 2, 4, 5), the model mean distributions are
 132 calculated from averaging the 160 year model results. In order to make comparisons with the
 133 40 years observation data, the error bars are calculated using the bootstrapping method. We did
 134 10,000 bootstrapping samples each selecting 480 months of data (i.e., 40 years) and calculated the
 135 average distribution of each sample. The error bars are calculated as the standard deviation over the
 136 10,000 40-year-equivalent averages. The distribution of the 10,000 averages is nearly Gaussian, so
 137 the standard deviation is an adequate measure of uncertainty.

138 For the ENSO variations section (Fig. 7, 8, 10), unlike the mean state uncertainties, the ENSO
 139 variations are interannual signals continuous in time. Their spectral analysis is most meaningful
 140 within a continuous decadal-scale period matching in duration to the available observational data.
 141 Thus, the 160 years of model results are divided into 4 non-overlapping sections of 40 continuous
 142 years. Corresponding distributions of each section are plotted as the thin, light lines, and the
 143 averaged values of the 4 sections are plotted as the thick, dark lines. Root-Mean Square Errors
 144 (RMSEs) are calculated between the averaged distributions and the observations.

145 To quantify the processes that influence the ENSO variation, we calculated the Bjerknes stability
 146 index (Jin et al. 2006) with the same equation as Zhao and Fedorov (2020).

$$2I_{BJ} = -\alpha_s - \frac{\langle \bar{u} \rangle}{L_x} - \frac{\langle -2y\bar{v} \rangle}{L_y^2} - \frac{\langle \mathcal{H}(\bar{w})\bar{w} \rangle}{H_m} + \mu_a\beta_u \left\langle \frac{\partial \bar{T}}{\partial x} \right\rangle + \mu_a\beta_w \left\langle \frac{\partial \bar{T}}{\partial z} \right\rangle + \mu_a\beta_h a_h \left\langle \frac{\bar{w}}{H_m} \right\rangle \quad (1)$$

147 The terms on the right hand side of this equation represent (1) Thermal Damping (TD), (2)
 148 the 2nd, 3rd, and 4th terms add up as the Mean Advection Damping (MA), (3) Zonal Advection
 149 Feedback (ZA), (4) Ekman Feedback (EK) and (5) Thermocline Feedback (TH). The first two
 150 mechanisms act as a damping effect on ENSO, while the remaining three feedback processes
 151 strengthen ENSO. This equation separates the different mechanisms that can influence the ENSO
 152 cycle, which allows us to understand what are key the processes that the Higher Andes experiment
 153 differs from the control experiment.

154 3. Changes in the mean state

155 Similar to the slab-ocean model simulations (Xu and Lee 2021), the Higher Andes in the
 156 atmosphere-ocean coupled model changes the mean state of the ocean and atmosphere. We will

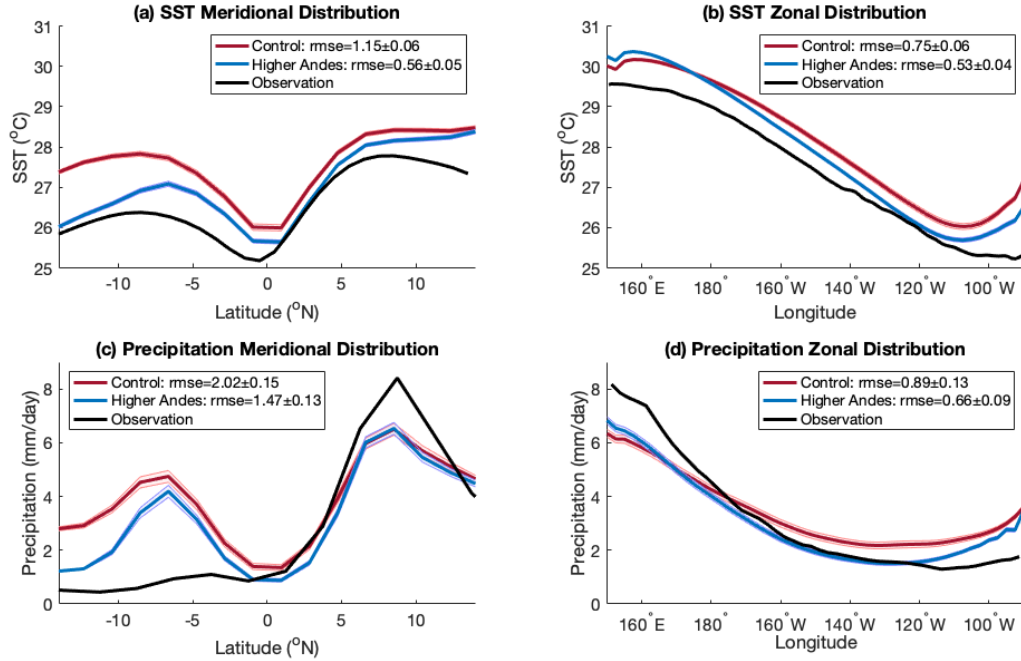
157 evaluate these changes in four aspects related to mean changes usually taken to affect ENSO: SST,
158 precipitation, wind stress and ocean stratification.

159 *a. SST and precipitation*

160 Bayr et al. (2018) and Wengel et al. (2018) found a link between the mean SST bias and
161 ENSO seasonality as well as the balance of mechanisms generating SST anomalies. As SST and
162 precipitation biases are linked (e.g. Oueslati and Bellon 2015; Brown et al. 2020), the effect of the
163 height of the Andes on these biases are analyzed together in this section.

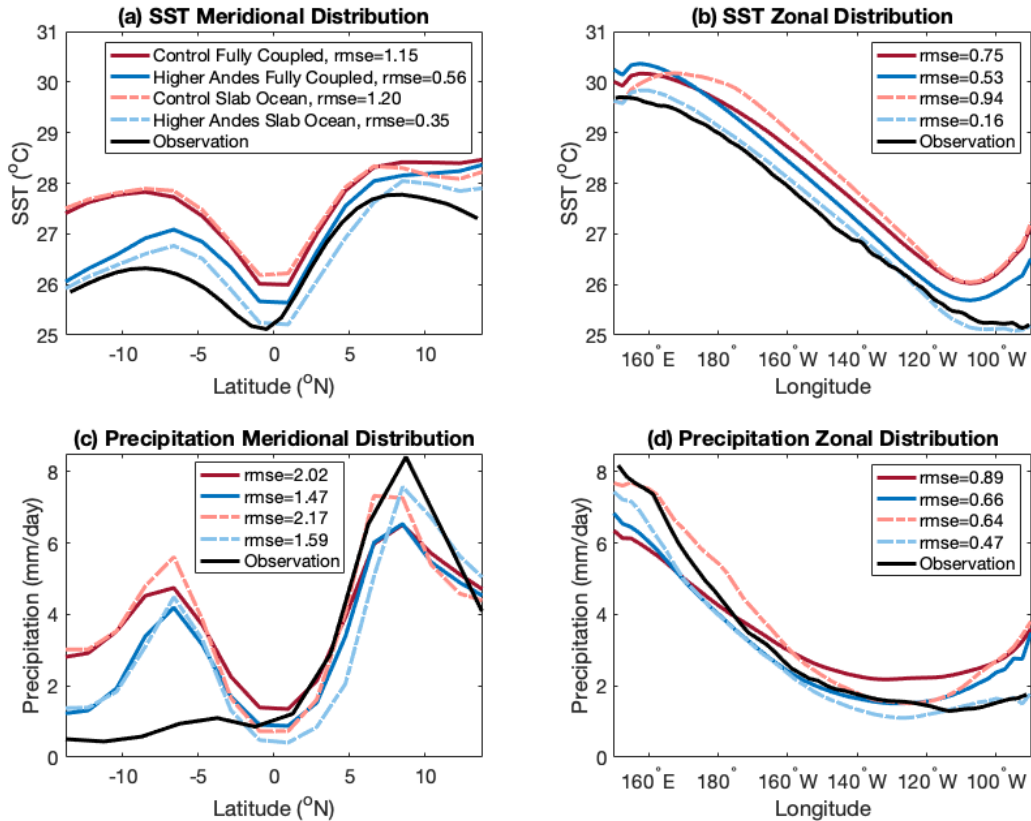
174 Figure 2 shows the latitudinal and longitudinal distribution of SST and precipitation in the
175 Observation (black line), Control (red line) and Higher Andes experiments (blue line). In the
176 eastern Pacific (Fig. 2a), the SST across latitudes is too warm in both experiments, but this warm
177 bias is smaller in the Higher Andes experiment than in the Control experiment (RMSE of 0.6 °C
178 and 1.2 °C respectively), especially south of the equator. As a consequence, the north-south (N-S)
179 SST gradient (defined as the difference between the highest SST in the northern and southern
180 hemisphere) is better reproduced in the Higher Andes experiment than in the Control experiment
181 (Higher Andes: 1.4 °C; Control: 0.7 °C; observation: 1.5 °C). Both experiments are also too
182 warm along the equator (Fig. 2b), but again, the bias is reduced in the Higher Andes experiment
183 compared to the Control experiment (RMSE of 0.5 °C and 0.8 °C respectively). Note that the bias
184 is reduced everywhere but west of the dateline.

185 In the tropical Pacific, the air from the southern and northern hemispheres converges. The
186 converged air is forced upward and creates the intertropical convergence zone (ITCZ), a region of
187 heavy precipitation, on average located at the north of the equator (Philander et al. 1996). The
188 observed precipitation distribution across latitudes in the eastern Pacific (Fig. 2c; black line)
189 displays a strong N-S precipitation difference, with around 1 mm/day south of the equator and
190 a peak reaching 8 mm/day around 7°N. In both experiments, the distribution of precipitation is
191 too symmetric with respect to the equator, a persistent error in climate models called the double
192 ITCZs bias (e.g., Lin 2007; Bellenger et al. 2014; Planton et al. 2021). The section-averaged bias is
193 around 2.0 mm/day in the Control experiment (red line), and N-S precipitation gradient (defined as
194 the difference between the largest precipitation in the northern and southern hemisphere) is around
195 2.1 mm/day. In the Higher Andes experiment, the double ITCZ bias is still present but reduced



164 FIG. 2. (a),(b) SST distribution in Observation, Control and Higher Andes experiments ($^{\circ}\text{C}$). (c),(d) Precip-
 165 itation distribution in Observation, Control and Higher Andes experiments (mm/day). (a),(c) are distributions
 166 across latitudes (zonal average 150°E - 90°W). (b),(d) are distributions along the equator (meridional average 5°S -
 167 5°N). The solid lines in model results are the averaged distribution over 160 years. The error bars are calculated
 168 with the bootstrapping method. We did 10,000 times of bootstrapping with 480 months (40 years) of data, and
 169 calculated the average distribution of each bootstrapping samples. The error bars are the standard deviations
 170 of these 10,000 average distributions. The observation distributions (black lines) are the average distribution of
 171 40 years. The legends also show the Root Mean Square Errors (RMSEs) calculated as the averaged difference
 172 between the model mean values (blue and red solid lines) and observations (black solid line). Uncertainties of
 173 the RMSEs are the averaged values of the error bars. See Method section for detailed explanations.

196 (the N-S precipitation difference of 2.4 mm/day), slightly reducing the mean bias (1.5 mm/day).
 197 However, increasing the height of the Andes does not improve the dry bias in the western equatorial
 198 Pacific, as shown in Fig. 2d. But it inhibits central and eastern tropical Pacific precipitation and
 199 still reduces the total precipitation bias (RMSE of 0.9 mm/day in the Control experiment and of
 200 0.7 mm/day in the Higher Andes experiment).

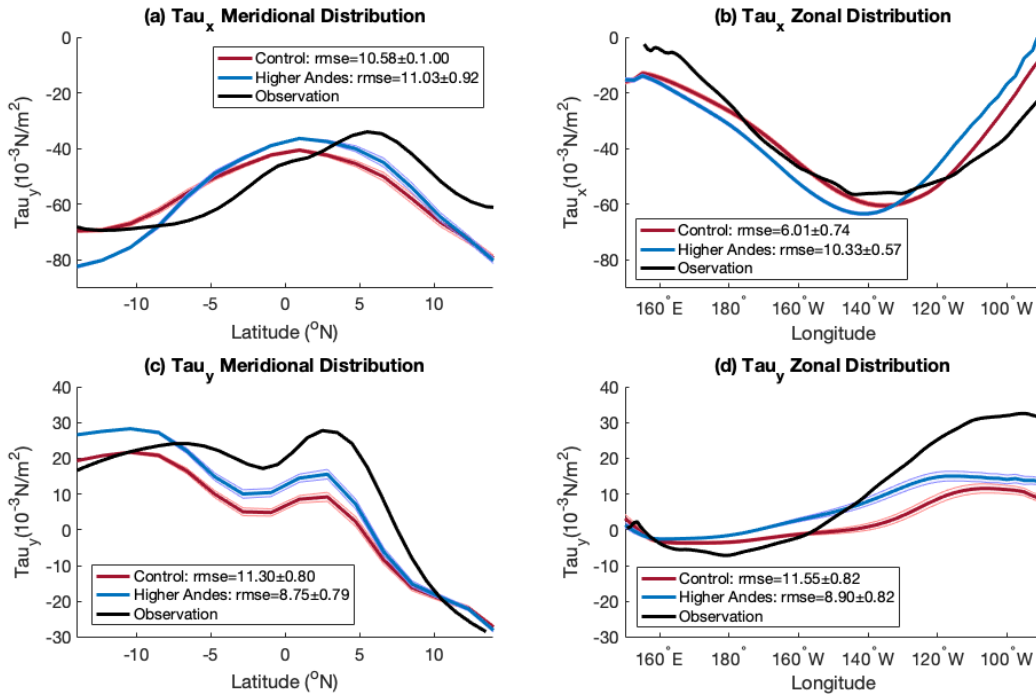


201 FIG. 3. Similar to Fig. 2, but for the comparison between fully-coupled model results (thick solid lines) and
 202 slab-ocean model results (thin dashed lines). The modeled fully-coupled distributions are averaged over the last
 203 160 years of 350 years simulations. The slab-ocean distributions are averaged over the last 10 years of 30 years
 204 simulations. Here we only showed the average distributions but not the error bars because the fully-coupled
 205 experiments and the slab-ocean experiments are run for different lengths compared with the observation. The
 206 legends also show the RMSEs calculated between the each modeled average values and observations.

207 The changes brought by the modification of the Andes are similar in the present experiment with
 208 a fully-coupled climate model and in the experiment from Xu and Lee (2021) with a slab ocean
 209 model (Fig. 3): a higher elevation of the Andes setting lowers the SST and reduces precipitation
 210 over the eastern tropical Pacific area. However, the difference between the Control and the Higher
 211 Andes experiments is smaller in the fully-coupled climate model, which means that the ocean
 212 circulation feedbacks respond to withstand the changes in the atmosphere, and end up weakening
 213 the influence from the Andes.

214 *b. Wind stress*

215 The surface wind over the tropical Pacific is an important factor that influences the heat and
 216 moisture transport, controls the coastal upwelling, and contributes to the development of the
 217 ENSO cycle (McPhaden et al. 2020). As both zonal and meridional wind stress modulate the
 218 amplitude of ENSO events (Hu and Fedorov 2018; Zhao and Fedorov 2020), we analyze their
 219 evolution between the two experiments in this section (Fig. 4).



220 FIG. 4. Same as Fig. 2, but for the zonal and meridional wind stress (10^{-3}N m^{-2}). In (a) and (c), zonal average
 221 is computed between 150°E and 270°E .

222 The tropical Pacific region, zonal wind stress is, on average, from east to west along the equator
 223 in the Pacific. The meridional component is northward in the southern hemisphere and up to
 224 7°N and southward in higher latitudes, to form the ITCZ (Fig. 4, black lines). This pattern is
 225 well reproduced in the Control experiment, but the cross-equatorial winds in the eastern equatorial
 226 Pacific are too weak (they reach $30 \times 10^{-3} \text{N m}^{-2}$ in the observation, but only $12 \times 10^{-3} \text{N m}^{-2}$ in
 227 the Control experiment; Fig. 4d).

228 With the Higher Andes experiment, zonal wind stress becomes stronger than in the Control
229 experiment and observations in the south Pacific (Fig. 4a) and in the central to western Pacific
230 region (Fig. 4b), and becomes weaker in the eastern Pacific region (Fig. 4b). As a consequence,
231 the zonal wind stress biases are slightly larger in the Higher Andes experiment than in the Control
232 experiment, across latitudes ($4.5 \times 10^{-3} \text{ N m}^{-2}$ and $2.7 \times 10^{-3} \text{ N m}^{-2}$ respectively) and along the
233 equator ($11.0 \times 10^{-3} \text{ N m}^{-2}$ and $6.7 \times 10^{-3} \text{ N m}^{-2}$ respectively). The meridional component does not
234 change much across latitudes (Fig. 4c). It becomes slightly too strong south of 5°S in the Higher
235 Andes experiment and gets closer to the observation in the equatorial band (5°S to 5°N). This does
236 not change the mean bias much (from $4.7 \times 10^{-3} \text{ N m}^{-2}$ in the Control experiment to $3.0 \times 10^{-3} \text{ N}$
237 m^{-2} in the Higher Andes experiment). Along the equator (Fig. 4d), there is little change west
238 of 200°E , but in the eastern equatorial Pacific, the cross-equatorial winds are strengthened in the
239 Higher Andes experiment, getting closer to the observation (but still too weak). This bias is slightly
240 improved but not by a lot (around $11.5 \times 10^{-3} \text{ N m}^{-2}$ in the Control experiment and around 8.9×10^{-3}
241 N m^{-2} in the Higher Andes experiment).

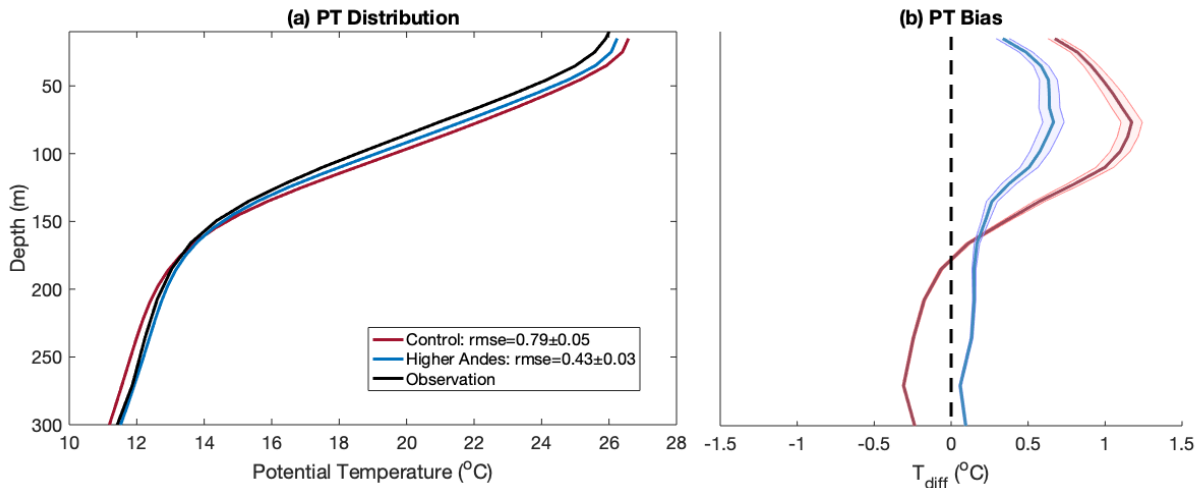
242 The modified atmospheric circulation is related to the change in SST. Similar to the slab ocean
243 model results from Xu and Lee (2021) (Fig. 3), the Higher Andes experiment lowers the SST in
244 the southeast Pacific by enhanced evaporative and radiative cooling (Xu and Lee 2021). The cooler
245 SST in the south Pacific will enhance the high sea surface pressure in the subtropical south Pacific,
246 and therefore enhance the anticyclonic motion (Takahashi and Battisti 2007). This enhanced
247 anticyclonic motion includes stronger easterly winds in the western equatorial Pacific (Fig.4b).
248 Also, the colder SST in the south Pacific increases the surface pressure gradient in the south and
249 the north Pacific, forming a stronger cross-equatorial wind from the southern hemisphere to the
250 northern hemisphere (Fig.4c). In conclusion, imposing a higher elevation of the Andes induces
251 stronger zonal and meridional wind stress in the tropical Pacific.

252 SST biases in different climate models are different (e.g. Fig.2 in Burls et al. 2017), but one
253 common problem is that the east-west SST gradient in the climate models is too small. The biases
254 are either a warm bias or a weaker cold bias in the eastern Pacific, indicating that the SST gradient
255 in most of the CMIP5 models is not as strong as in the observations. Our experiment increases the
256 east-west SST gradient by elevating the height of the Andes, and this change is accompanied by
257 stronger winds over the tropical Pacific.

258 *c. Ocean stratification*

259 Because the Higher Andes setting changes the atmosphere circulation, the upper ocean would
 260 respond to this change and reach a new equilibrium. Here we show the upper ocean temperature
 261 distribution in the two experiments from years 191 to 350. An important aspect of the signal that
 262 develops into an ENSO event is the propagation of a temperature anomaly in the subsurface ocean,
 263 and it can be measured by the change of thermocline depth (e.g., Zhao and Fedorov 2020).

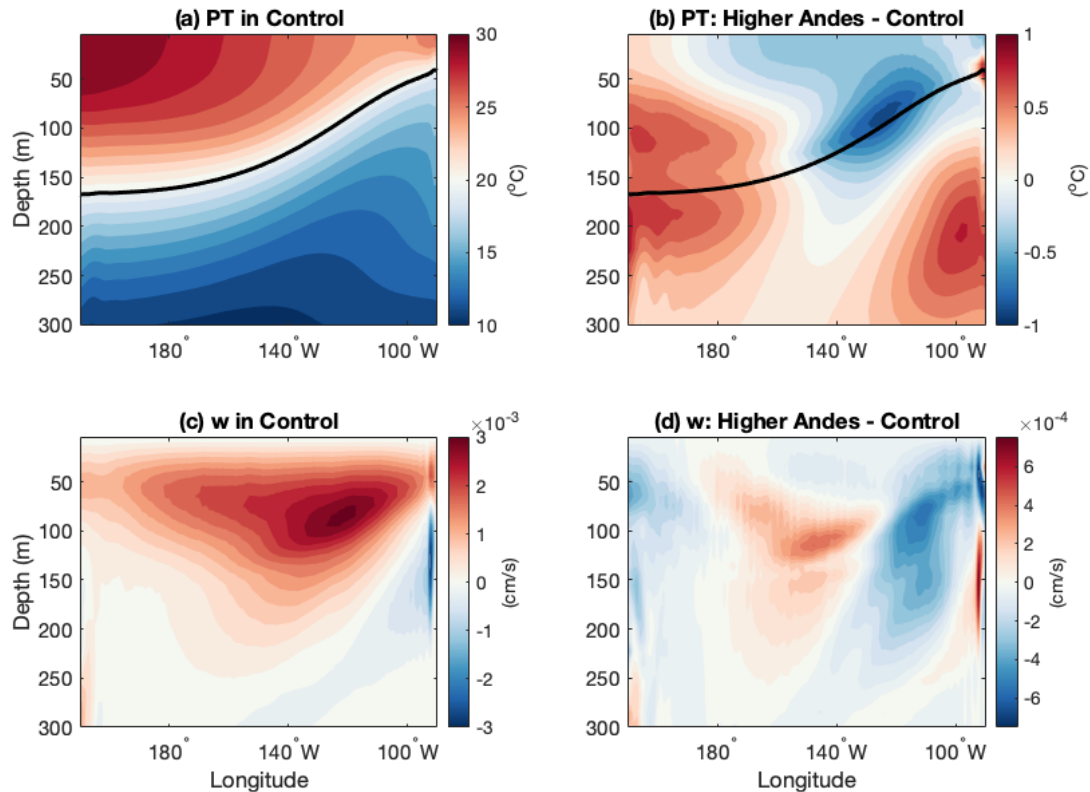
264 Fig. 5 shows the potential temperature distribution in NINO3 region (150° – 90° W, 5° S– 5° N) in
 265 both experiments and in the observations (left panel), as well as the differences between the model
 266 and the observations (right panel). The Higher Andes experiment is closer to the observations, being
 267 colder than the Control experiment in the upper 150 m and warmer than the Control experiment
 268 from 150 m to 300 m. As shown in Fig. 5, compared with the Higher Andes experiment, the
 269 Control experiment has a too large vertical temperature gradient in the NINO3 region, implying
 270 too strong stratification.



271 FIG. 5. (a) Vertical distribution of the potential temperature (PT, °C) averaged over the NINO3 region (210-
 272 270°E, 5° S- 5° N). (b) Biases of PT in the vertical distribution over the NINO3 region (model experiments minus
 273 observations). Error bars are calculated with a similar method as Fig. 2.

274 Fig. 6a,b show the vertical distribution and the change of potential temperature in the upper
 275 ocean of the equatorial Pacific. The thermocline in the Pacific ocean is tilted (black line in Fig
 276 6a); it is deeper in the western Pacific and shallower in the eastern Pacific. A cooler potential
 277 temperature indicates a shallower thermocline, while a warmer potential temperature indicates a

278 deeper thermocline. The Higher Andes experiment imposes a cooling in the eastern part of the
 279 thermocline, and a warming in the western part (Fig. 6b), indicating a shallower thermocline in
 280 the east and deeper in the west, resulting in a more zonal thermocline tilt.



281 FIG. 6. (a) Vertical PT distribution at the equator for Control experiment ($^{\circ}\text{C}$), the black line representing the
 282 depth of the 20°C isotherm (Z20). (b) PT distribution for Higher Andes minus Control ($^{\circ}\text{C}$), with the black line
 283 representing the same Z20 as in (a). (c) Vertical velocity (w , cm/s) for Control experiment.. (d) Vertical velocity
 284 (cm/s) for Higher Andes minus Control.

285 However, this change in upper ocean potential temperature is not driven by stronger coastal
 286 upwelling. In the eastern equatorial Pacific, the upper ocean is dominated by strong upward
 287 motion (Fig. 6c), but in the Higher Andes, upwelling weakens due to the weaker zonal wind stress
 288 in the eastern Pacific (Fig. 4b).

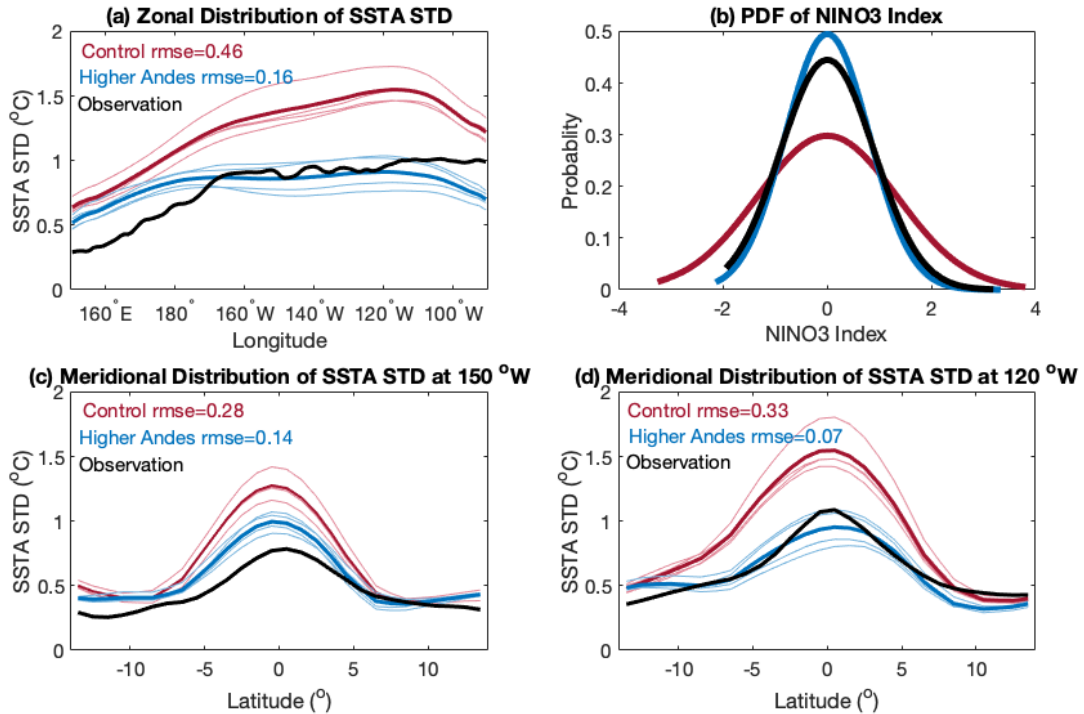
289 **4. Changes in ENSO Properties**

290 As the mean state climate over the tropical Pacific is thought to be related to the ENSO variability
291 (Zhao and Fedorov 2020), the modification of the Andes is expected to influence the ENSO cycle.
292 The long-term changes in ocean mean state climate are the results of the changes in ENSO, as
293 was suggested by Atwood et al. (2017). In the periods during which ENSO has an unusually
294 large amplitude, the mean state climate will have cooler SSTs in the eastern Pacific and stronger
295 precipitation in the western Pacific, which tends to damp ENSO variability. In fact, the changes
296 in the mean state can affect the major feedbacks that control the characteristics of the ENSO cycle
297 (Karamperidou et al. 2020). Therefore, in this section, we will evaluate ENSO performance in the
298 Higher Andes experiment from various characteristics of the ENSO cycle.

299 *a. Amplitude*

300 Fig. 7a shows the zonal distribution of the standard deviation (STD) of SST anomalies (SSTA)
301 over the equatorial Pacific. The observation exhibits a small variability in the western Pacific region
302 but from 190°E to the South American coast, the SSTA has a near-constant STD of about 0.9 °C. In
303 the Control experiment, the SSTA STD is around 0.5 °C larger than observed all along the equator.
304 The simulated SSTA variability also peaks clearly around 245°E before decreasing towards the
305 South American coast. With the Higher Andes setting, the SSTA variability is decreased all over
306 the equatorial Pacific, resulting in a similar amplitude of SSTA STD to the observation from 190°E
307 to 240°E. The differences in the variability strength is consistent with changes in the NINO3 index
308 probability distribution function (PDF) (Fig. 7b). In the Control experiment, extreme El Niño and
309 La Niña events happen more frequently than the observations. But in the Higher Andes experiment,
310 the distribution gets more concentrated to the center and the shape of its PDF is more similar to the
311 observation. Although SSTA variability is still too high in the western equatorial Pacific and now
312 has a too low variability in the far eastern Pacific in the Higher Andes experiment, its RMSE is
313 still much smaller than the Control experiment. Overall, the Higher Andes experiment captures a
314 much weaker SSTA variability over the equatorial Pacific compared with the Control experiment,
315 more consistent with the observed variability.

322 Fig. 7c and d show the meridional SSTA STD distributions in the central (150°W) and eastern
323 (240°E) Pacific. In the central Pacific, the Control SSTA variations are much stronger than the



316 FIG. 7. (a) Standard deviation (STD) of SST anomaly (SSTA) along the equator ($^{\circ}\text{C}$; 5°S - 5°N average). (b)
 317 Probability Distribution Function (PDF) of NINO3 index. (c),(d) meridional distribution of SSTA STD ($^{\circ}$) at
 318 150°W and 120°W . The 160 year model results are divided into 4 sections of 40 years. Distributions of each
 319 section are plotted as thin, light lines and the averaged values of the 4 non-overlapping sections are plotted as thick,
 320 dark lines. The legends also show RMSEs calculated between the averaged distributions and the observations.
 321 See Method section for detailed explanations.

324 observation from the 5°S to 5°N region, with an error of 0.5°C at the equator (66% stronger
 325 than the observation). By adjusting the Andes, the difference from the observation is reduced
 326 by more than a half and is now down to 0.2°C larger than observed. In the eastern Pacific, the
 327 Control experiment has also a too large STD. With Higher Andes the STD is much reduced and the
 328 observation falls within uncertainties (blue shading in Fig. 7d). The comparison of the meridional
 329 distribution demonstrates that the Higher Andes experiment largely improves the SSTA variation
 330 errors near the equator.

331 In the NINO3 region, the Higher Andes experiment has slightly weaker SSTA STD (0.8°C)
 332 compared to the observation (1.0°C), while the Control experiment variation is about 50% stronger

333 than the observation (1.5 °C). The distribution of SSTA in the NINO3 region is quite narrow in the
 334 observation, with 90% of the SSTA being moderate or neutral SSTA (NINO3 SSTA between -1.5
 335 °C and +1.5 °C). The distribution in the Control experiment is too spread out, with only 72% of
 336 moderate or neutral SSTA. In this aspect, the Higher Andes experiment is closer to the observation
 337 (94% of moderate or neutral SSTA). The meridional distribution of SSTA is closely related to the
 338 frequency of ENSO and the meridional span of the anomalous Bjerknes feedback (e.g., Neale et al.
 339 2008).

340 Fig. 8 shows the seasonality of the ENSO variations. ENSO variability peaks during boreal
 341 winter and is weakest during boreal spring. This pattern is reproduced by both experiments but
 342 the intensity of the variability is too high in the Control experiment and is mostly correct in the
 343 Higher Andes experiment (within the observed values; blue lines). A closer analysis shows that the
 344 intensity of the seasonality (defined as the variability during November-January divided by March-
 345 May) is slightly increased in the Higher Andes experiment compared to the Control experiment
 346 and is closer to the observation (NINO3.4 region ((5°N-5°S, 170°W-120°W): 1.4 (Higher Andes),
 347 1.3 (Control) and 1.7 (Observation); NINO3 region: 1.2 (Higher Andes), 1.2 (Control) and 1.7
 348 (Observation)).

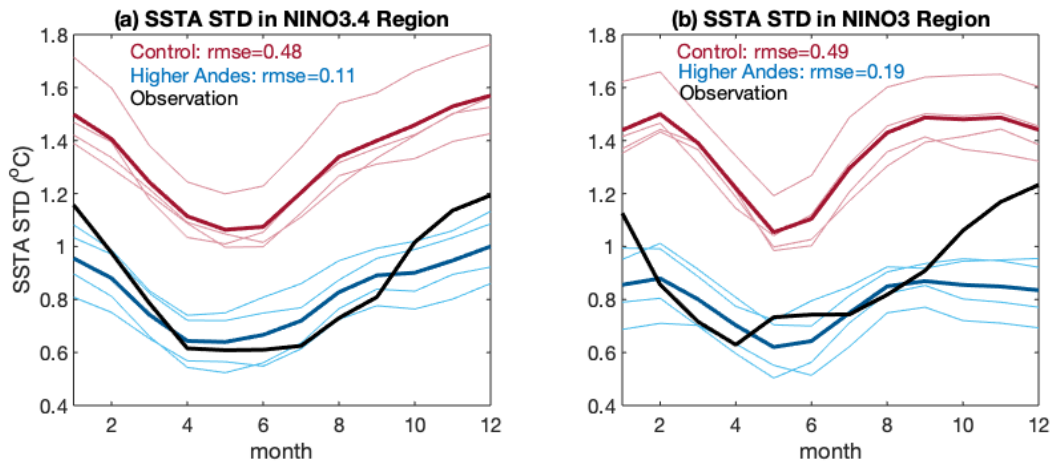


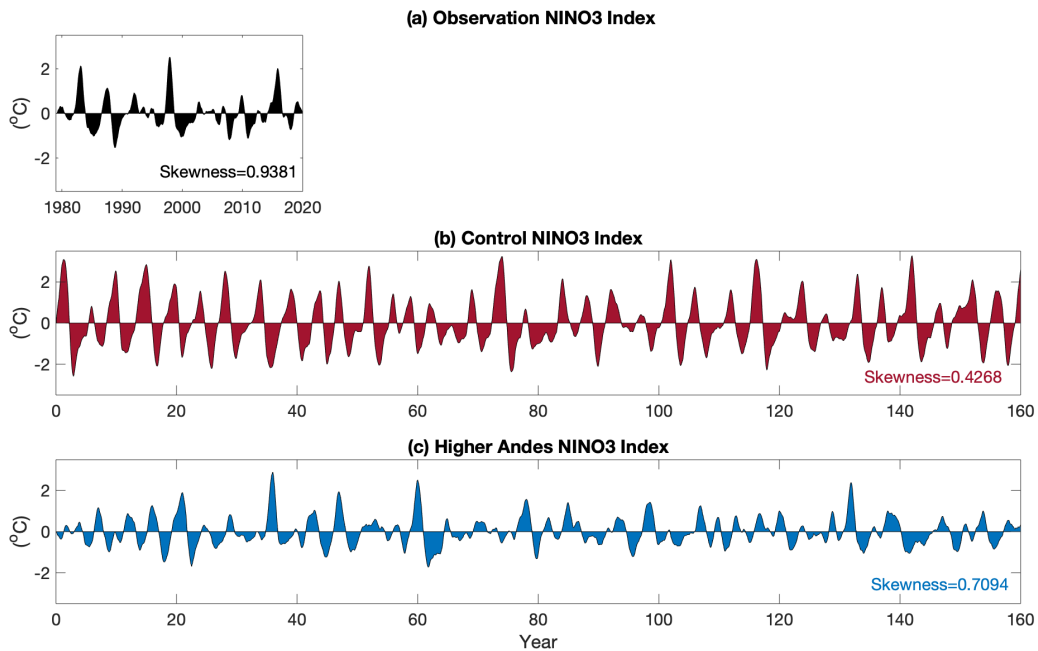
FIG. 8. Seasonal evolution of SSTA STD (°) in (a) NINO3.4 region and (b) NINO3 region.

349 *b. Skewness*

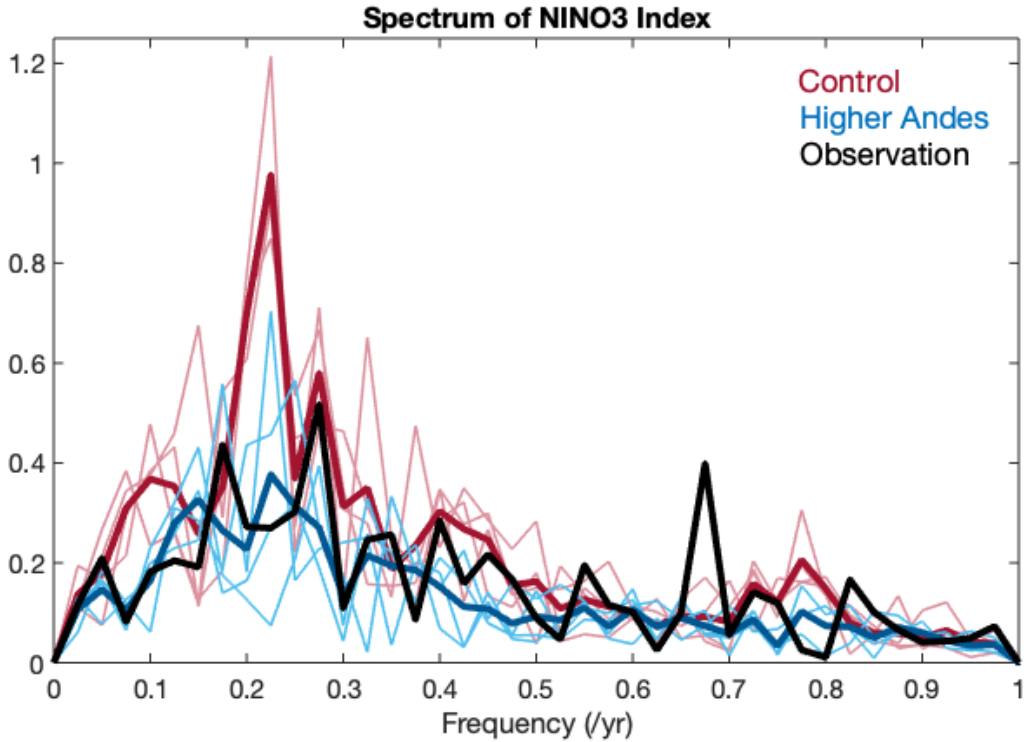
350 The SSTA skewness is a key measurement of the ENSO asymmetry, which is produced by the
 351 nonlinear processes in the ENSO cycle (e.g., An et al. 2020). In the eastern Pacific NINO3 region,

352 the SSTA skewness is strongly positive (Dommenget et al. 2013), meaning that El Niño events can
353 reach larger amplitudes than La Niña events, but occurring less frequently.

354 Similar to Kohyama et al. (2017), we calculated the skewness of the 11-month running mean
355 NINO3 SSTA (Fig. 9a), and find a value of 0.9. The same method is applied to the Control
356 (Fig.9b) and Higher Andes (Fig. 9c) experiments. In the control experiment, the skewness is less
357 than half of the observed (0.4), suggesting that the El Niño and La Niña events are too similar in
358 amplitude. In the Higher Andes experiment, the skewness (0.7) is still too weak but much closer
359 to the observed value. The calculation of the skewness is consistent with the changes in the PDF
360 of the experiments (Fig. 7b). The variation in the observations ranges from -1.94 °C to 3.19 °C. In
361 the Control experiment, the range is -3.26 °C to 3.81 °C, while in the Higher Andes experiment it
362 is -2.14 °C to 3.33 °C. Thus, the Higher Andes experiment captures a more similar variation range
363 and the asymmetry between positive and negative phases.



364 FIG. 9. Time series of 11-month running mean Niño3 index, as Kohyama et al. (2017), for (a) observations,
365 (b) Control and (c) Higher Andes. Skewness of the distributions indicated at the bottom right of each panel.



367 FIG. 10. Normalized spectrum of Niño3 index. The 160 year model results are divided into 4 non-overlapping
 368 sections of 40 years. Spectrum of each section is plotted as thin, light line and the averaged value of the 4 sections
 369 is plotted as thick, bold lines. See Method section for detailed explanations.

366 *c. Spectral Characteristics*

370 The spectra of the NINO3 index can reveal the variability across time scales of the ENSO cycle
 371 (Guilyardi et al. 2009). In the spectrum of the observed NINO3 index time series, the strongest
 372 signal is at 0.27 /yr, which is a 3.7 years cycle but even with this strongest signal, its normalized
 373 amplitude is only 0.51. The dominant ENSO cycle does not have a very strong signal at a particular
 374 frequency; instead, the ENSO cycle is somewhat irregular and its period is around 4 years.

375 To perform a spectral analysis with uncertainties appropriate for comparison to the observed
 376 40-year record, we used 160 years of data split into 4 sections of 40-years spans of data. The
 377 spectrum is calculated for each section (light lines) and then the average at each frequency (bold
 378 lines) for the Control and Higher Andes experiments (Fig. 10) are shown. The Control experiment
 379 spectrum has an excessive peak at the frequency of 0.22/yr, revealing its very strong periodic
 380 4.5-year cycle, which is contradictory to the observation. A weaker peak near a 10 year period is

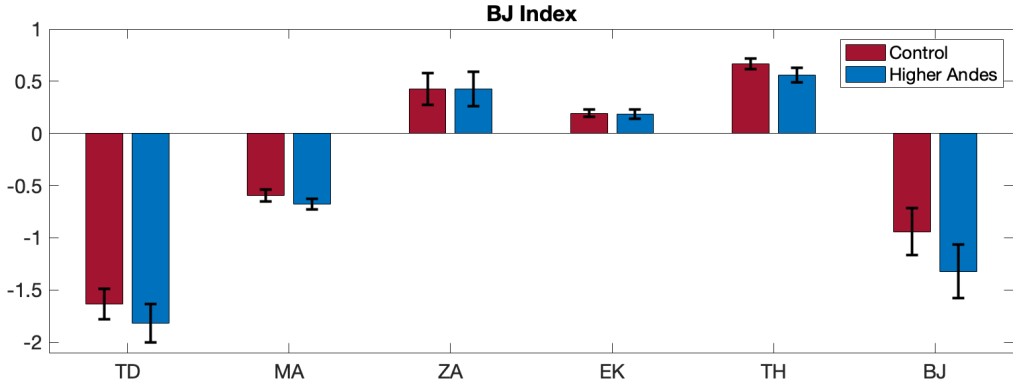
381 also present in the Control experiment, but not in the observation. In the Higher Andes experiment,
382 the 4.5-year and 10-year peaks disappear and the spectrum more realistically captures a 3 to 8 year
383 irregular, broadband ENSO cycles. Although the amplitude of the Higher Andes experiment is
384 slightly weaker than the observed spectrum, the observed spectrum falls within the error bars of the
385 Higher Andes experiment in most of the frequencies between 0.1 and 0.4. At higher frequencies
386 (0.5 cycles/year and above), the observations and both simulations agree. The irregularity of ENSO
387 over its dominant frequency range is therefore much improved in the Higher Andes experiment.

388 **5. Mechanism**

389 The modification of the Andes results in a more La Niña-like oceanic mean state (steeper ther-
390 mocline tilt, colder eastern Pacific surface waters, enhanced eastern Pacific zonal and meridional
391 wind stresses), accompanied by fewer, less periodic, meridionally narrower, and less extreme
392 ENSO events with greater asymmetry between El Niño and La Niña. For the changes in the mean
393 state, the mechanisms are similar to what has been discussed in Xu and Lee (2021), with the
394 additional influence of ocean dynamical processes, especially upwelling and horizontal advection.
395 A higher elevation of the Andes has a stronger effect in squeezing the isentropic layers in the
396 atmosphere compared with the Control experiment. As a result, when the mid-latitude westerly
397 wind approaches the Andes, it becomes more difficult for the air mass to cross the mountains
398 so the wind turns equatorward. This equatorward turning is accompanied by downward motion
399 because of conservation of potential vorticity. With the strengthening of the anticyclonic motion
400 in the southeast Pacific associated with this equatorward turning, the atmosphere will have lower
401 specific humidity and stronger latent heat uptake, enhancing the formation of the low-level clouds
402 above the ocean. These low-level clouds will block the shortwave radiation and further lower the
403 SST in a positive feedback (Takahashi and Battisti 2007). The thermocline becomes more tilted
404 and the eastern upper Pacific less stratified. The ocean upwelling is weaker in the eastern Pacific
405 and stronger in the central Pacific, consistent with the change in zonal wind stress. These changes
406 in the Higher Andes experiment are correlated with the ENSO variations, either by changing the
407 mean state feedback or by changing the strength of the correlation between anomalies.

408 We calculated the Bjerknes Index (BJ) as Eq. 1 (Fig. 11), where uncertainty in each terms is
409 estimated based on 1000 samples using Bootstrapping method. Detailed comparisons for each term

410 are shown in Table 1. Results indicate that the reason for the weaker ENSO in the Higher Andes
 411 experiment is the stronger damping effect from the mean state. Among the contributions from the
 412 different terms, the difference is mainly due to the stronger Thermal Damping, the stronger Mean
 413 Advection Damping and the weaker Thermocline feedback.



414 FIG. 11. BJ Index in both experiments. TD: Thermal Damping. MA: Mean Advection damping. ZA: Zonal
 415 Advection feedback. EK: Ekman feedback. TH: Thermocline feedback. BJ: BJ Index, sum of all the previous
 416 terms. The error bars represent 95% confidence level. They are obtained by bootstrapping of the original data
 417 1000 times, calculating the corresponding BJ indexes with each bootstrapping sample, then compute the standard
 418 deviations of each term.

422 The thermal damping term is the linear regression between the surface energy flux anomaly and
 423 the eastern Pacific SST anomaly. The surface energy flux depends negatively on the regional SST,
 424 and in the Higher Andes experiment this regression has a steeper slope. According to Kim et al.
 425 (2014), this atmospheric feedback is underestimated in the CMIP3 and CMIP5 models. In our
 426 experiment, the changes in the regression are mainly contributed by the change in latent heat flux
 427 (Table 1). The Higher Andes experiment has stronger downward motion of the air over the southeast
 428 Pacific with lowered specific humidity, inducing stronger evaporation and takes up more latent heat
 429 flux from the ocean surface. The stronger latent heat flux contributes to a stronger thermal damping.
 430 However, this term, estimated by linear regression, has a relatively large uncertainty related to the
 431 fact that the thermal damping includes some nonlinear feedback including the subsidence response
 432 to SST and the high-level cloud cover. Thus, thermal damping is only moderately stronger in the
 433 Higher Andes experiment than in the Control experiment.

Name	Decomposition of the Term	Definition	Control	Higher Andes
TD	$-\alpha_s$	$Q_s = -\alpha_s \langle T' \rangle$	-1.64	-1.82
	* $-\alpha_{SW}$	$SW_s = -\alpha_{SW} \langle T' \rangle$	-0.40	-0.23
	* $-\alpha_{LW}$	$LW_s = -\alpha_{LW} \langle T' \rangle$	-0.05	-0.05
	* $-\alpha_{LH}$	$LH_s = -\alpha_{LH} \langle T' \rangle$	-1.08	-1.41
	* $-\alpha_{SH}$	$SH_s = -\alpha_{SH} \langle T' \rangle$	-0.12	-0.13
MA	Udamp	$-\frac{\langle \bar{u} \rangle}{L_x}$	0.36	0.26
	Vdamp	$-\frac{\langle -2y\bar{v} \rangle}{L_y^2}$	0.49	0.46
	Wdamp	$-\frac{\langle \mathcal{H}(\bar{w})\bar{w} \rangle}{H_m}$	-1.45	-1.40
ZA			0.43	0.44
	μ_a	$[\tau'_x] = \mu_a \langle T' \rangle$	5.36e-3	5.29e-3
	β_u	$\langle u' \rangle = \beta_u [\tau'_x]$	4.26	4.85
	$\langle \frac{\partial \bar{T}}{\partial x} \rangle \times C_{time}$		18.63	16.97
EK			0.20	0.19
	μ_a	$[\tau'_x] = \mu_a \langle T' \rangle$	5.36e-3	5.29e-3
	β_w	$\langle \mathcal{H}(\bar{w})w' \rangle = -\beta_w [\tau'_x]$	2.50e-5	2.37e-5
	$\langle \frac{\partial \bar{T}}{\partial z} \rangle \times C_{time}$		1.46e+6	1.50e+6
TH			0.67	0.56
	μ_a	$[\tau'_x] = \mu_a \langle T' \rangle$	5.36e-3	5.29e-3
	β_h	$\langle h' \rangle = \beta_h [\tau'_x]$	5.71	5.09
	a_h	$\langle \mathcal{H}(\bar{w})T'_{50m} \rangle = a_h \langle h' \rangle$	17.93	17.44
	$\langle \frac{\bar{w}}{H_m} \rangle \times C_{time}$		1.22	1.19
BJ			-0.94	-1.31

419 TABLE 1. BJ index equation (Eq. 1) terms comparison. Terms with bold text are not overlapping in 33% - 67%
420 range (1 STD) between the two experiments, which means the change is significant. '*' represents terms that are
421 not directly included in the BJ index equation. C_{time} is the time constant that converts the unit from s^{-1} to yr^{-1} .

434 The second term that contributes to the stronger damping BJ index is the mean advection
435 damping. Among the three directions, the zonal and meridional mean currents are positive
436 feedback that strengthens the ENSO cycle, but the vertical current has a much stronger negative
437 effect. In the comparison between the Control and the Higher Andes experiments, the changes in
438 all three dimensions are significant (Table. 1). The weaker zonal mean current feedback is the
439 main contributing term for the difference between Higher Andes and Control experiments. In the
440 Higher Andes experiment, the mean westward current velocity in the NINO3 region within the
441 mixed layer decreases from 5.4 cm/s to 3.5 cm/s (36% decrease). This change is consistent with
442 the weaker zonal wind stress in the eastern tropical Pacific region (Fig. 4b).

443 The third term that contributes the the stronger damping is the weakened Thermocline feedback
444 in the Higher Andes experiment. The thermocline feedback quantifies the influence from the
445 thermocline depth anomaly to the eastern Pacific surface temperature anomaly. In the Higher
446 Andes experiment, the eastern Pacific becomes colder and the mean thermocline becomes deeper
447 (Fig. 6. As a result, the upper ocean is less stratified in the NINO3 region (Fig. 5). When the
448 eastern equatorial Pacific becomes less stratified, the zonal thermocline slope is less sensitive to
449 the wind stress (Kim et al. 2014) (β_h in Table 1). With the weaker oceanic response to the wind
450 anomaly in the Higher Andes experiment, the Thermocline Feedback becomes weaker and results
451 in a weaker ENSO cycle.

452 Combining all the terms of the BJ index, the average damping index changed by 38%, from -0.94
453 in the Control experiment to -1.31 in the Higher Andes experiment. Therefore, it is very likely
454 that the ENSO amplitude is weaker in the Higher Andes experiment because of the stronger overall
455 damping effect.

456 **6. Conclusion**

457 In this study, we performed an experiment to understand how the simulated height of the Andes
458 affects the Pacific climate of the CESM atmosphere-ocean global coupled model. The results show
459 that by elevating the height of the Andes, the model simulates the tropical Pacific mean state climate
460 and the ENSO variations better, which suggests that creating elevation maps by simply smoothing
461 away the high and low features of high resolution observations is an oversimplification. For the
462 mean state climate, the Higher Andes experiment results in a greater east-west and north-south
463 SST gradient, and reduced precipitation over the south Pacific. Easterly wind stress in the eastern
464 and central Pacific becomes stronger, accompanied by stronger cross-equator southerly wind stress.
465 In the upper ocean, the Higher Andes experiment is less stratified over the eastern tropical Pacific,
466 and it has a steeper east-west thermocline slope. ENSO variability is strongly affected: the Higher
467 Andes experiment exhibits a smaller amplitude, a greater skewness and a less regular ENSO period.
468 All of these changes exceeded the uncertainty due to limited simulation length, and all are more
469 consistent with observations results. Therefore, in this version of CESM a higher elevation of the
470 Andes allows better simulation of the tropical Pacific mean state as well as ENSO variations in the
471 CESM coupled model.

472 Although the improvement in the mean state climate and the ENSO properties are related, it
473 is hard to distinguish cause and effect. On the one hand, the changes in the climate mean state
474 can influence the ENSO characteristics (e.g., Fedorov and Philander 2000; Hu and Fedorov 2018;
475 Zhao and Fedorov 2020). Zhao and Fedorov (2020), suggesting that strengthening of thermocline
476 stratification and deepening the mean thermocline depth will produce stronger ENSO. In our
477 simulations, the Higher Andes experiment has a weaker upper ocean stratification and a shallower
478 thermocline depth over the central and eastern Pacific (Fig. 6), and we found a consistent change
479 toward weaker ENSO events (Fig. 7). In addition, Hu and Fedorov (2018) suggests that with a
480 stronger zonal wind over the central-western Pacific and stronger cross-equatorial winds over the
481 eastern Pacific, there will be a weaker amplitude of ENSO variations. Consistently, our results also
482 suggest that the elevation of the Andes strengthens the wind and weakens ENSO variability. On
483 the other hand, the changes in the ENSO variations can also influence the tropical Pacific mean
484 state. Because of the asymmetry of El Niño and La Niña, the changes of the mean state can result
485 from the varying occurrence and strength of strong El Niño and La Niña events, and the residual
486 between them (Rodgers et al. 2004; McPhaden et al. 2011; Atwood et al. 2017). In our result, the
487 Higher Andes experiment significantly reduces the occurrence of strong El Niño events, but has a
488 smaller influence on the La Niña events (Fig. 9). As a result, the eastern Pacific will have a cooler
489 mean state in the Higher Andes case.

490 Feng and Poulsen (2014) performed a similar experiment of modifying the height of the Andes in
491 a similar global coupled climate model (CCSM4), and examined the response of the Pacific climate.
492 However, their purpose was to understand the impact of Andean uplift over geological time, while
493 our purpose was to understand biases in the modern Pacific climate and ENSO. Furthermore, the
494 details of how the Andes were changed and thus the results are quite different. Feng and Poulsen
495 (2014) carried out their experiment to understand if the long-term climate transition in the Pacific
496 since late Cenozoic is the result from the from 1 to 3 km kilometer-scale uplift of the central Andes.
497 Our experiment is seeking an appropriate representation of the Andes in global climate models
498 for the present day (changing the maximum elevation from about 2 km to about 5 km), so as to
499 understand the model biases in the Pacific climate simulation. With this purpose, we compare our
500 results against observations to evaluate the simulation's performance. In addition, the resulting
501 changes in ENSO here are distinct from Feng and Poulsen (2014). In their experiment, as the

502 height of the Andes increases, the ENSO period decreases. In comparison, here no obvious change
503 in the dominant frequency occurs, but the strength of the NINO3 index spectral band reduces in
504 our Higher Andes experiment (Fig. 10). In their histogram of ENSO events, they have slightly
505 more extreme El Niño and La Niña events, less moderate El Niño and La Niña events and more
506 weak El Niño and La Niña events in the Higher Andes experiment. In our result, both extreme
507 and moderate El Niño and La Niña events decreased in frequency in the Higher Andes experiment
508 (Fig.7b), and phase asymmetry increased. However, consistent with our results, they find that the
509 mean zonal SST gradient increased with increasing the height of the Andes, although more so than
510 in our experiment. They found major strengthening of zonal winds while we find modest changes
511 to the mean wind magnitude and structure.

512 Overall, we consider the modification of the Andes an improvement in representing the South
513 American topography and the tropical Pacific mean climate and its variability. This work highlights
514 the fact that increasing the resolution of a climate model without addressing the height of the Andes
515 could be problematic.

516 *Acknowledgments.* We want to thank Dr. Alexey Fedorov, Anson Cheung, Mengxi Wu for their
517 comments and suggestions on this research. The constructive comments from three anonymous
518 reviewer are also greatly appreciated. The runs are performed on the Brown Ocean State Center for
519 Advanced Resources (OSCAR). We want to thank Institute at Brown for Environment and Society
520 (IBES) for supporting this project on the AGU 2022 Ocean Science presentation. BFK was
521 supported by ONR N00014-17-1-2393. MJM is supported by NOAA's Global Ocean Monitoring
522 and Observing Program. PMEL contribution no. 5304.

523 *Data availability statement.* Model results are available at <https://doi.org/10.7910/DVN/3H1E4X>.

524 **References**

- 525 Abellán, E., S. McGregor, and M. H. England, 2017: Analysis of the Southward Wind Shift of
526 ENSO in CMIP5 Models. *Journal of Climate*, **30** (7), 2415–2435, doi:10.1175/JCLI-D-16-0326.
527 1, URL <https://journals.ametsoc.org/view/journals/clim/30/7/jcli-d-16-0326.1.xml>, publisher:
528 American Meteorological Society Section: Journal of Climate.
- 529 Adler, R. F., and Coauthors, 2003: The Version-2 Global Precipitation Climatology Project (GPCP)
530 Monthly Precipitation Analysis (1979–Present). *Journal of Hydrometeorology*, **4** (6), 1147–

531 1167, doi:10.1175/1525-7541(2003)004<1147:TVGPCP>2.0.CO;2, URL https://journals.ametsoc.org/view/journals/hydr/4/6/1525-7541_2003_004_1147_tvGPCP_2_0_co_2.xml, publisher: American Meteorological Society Section: Journal of Hydrometeorology.

532
533

534 An, S.-I., E. Tziperman, Y. M. Okumura, and T. Li, 2020: ENSO Irregularity and Asymmetry. *El Niño Southern Oscillation in a Changing Climate*, American Geophysical Union (AGU), 153–172, doi:10.1002/9781119548164.ch7, URL <https://agupubs.onlinelibrary.wiley.com/doi/abs/10.1002/9781119548164.ch7>, section: 7 _eprint: <https://agupubs.onlinelibrary.wiley.com/doi/pdf/10.1002/9781119548164.ch7>.

535
536
537
538

539 Atwood, A. R., D. S. Battisti, A. T. Wittenberg, W. H. G. Roberts, and D. J. Vimont, 2017: Characterizing unforced multi-decadal variability of ENSO: a case study with the GFDL CM2.1 coupled GCM. *Clim Dyn*, **49** (7), 2845–2862, doi:10.1007/s00382-016-3477-9, URL <https://doi.org/10.1007/s00382-016-3477-9>.

540
541
542

543 Bastianin, A., A. Lanza, and M. Manera, 2018: Economic impacts of El Niño southern oscillation: evidence from the Colombian coffee market. *Agricultural Economics*, **49** (5), 623–633, doi:10.1111/agec.12447, URL <https://onlinelibrary.wiley.com/doi/abs/10.1111/agec.12447>, _eprint: <https://onlinelibrary.wiley.com/doi/pdf/10.1111/agec.12447>.

544
545
546

547 Bayr, T., M. Latif, D. Dommenges, C. Wengel, J. Harlaß, and W. Park, 2018: Mean-state dependence of ENSO atmospheric feedbacks in climate models. *Clim Dyn*, **50** (9), 3171–3194, doi:10.1007/s00382-017-3799-2, URL <https://doi.org/10.1007/s00382-017-3799-2>.

548
549

550 Bellenger, H., E. Guilyardi, J. Leloup, M. Lengaigne, and J. Vialard, 2014: ENSO representation in climate models: from CMIP3 to CMIP5. *Clim Dyn*, **42** (7), 1999–2018, doi:10.1007/s00382-013-1783-z, URL <https://doi.org/10.1007/s00382-013-1783-z>.

551
552

553 Bjerknes, J., 1969: ATMOSPHERIC TELECONNECTIONS FROM THE EQUATORIAL PACIFIC. *Monthly Weather Review*, **97** (3), 163–172, doi:10.1175/1520-0493(1969)097<0163:ATFTEP>2.3.CO;2, URL https://journals.ametsoc.org/view/journals/mwre/97/3/1520-0493_1969_097_0163_atftep_2_3_co_2.xml, publisher: American Meteorological Society Section: Monthly Weather Review.

554
555
556
557

- 558 Boos, W. R., and Z. Kuang, 2010: Dominant control of the South Asian monsoon by orographic
559 insulation versus plateau heating. *Nature*, **463 (7278)**, 218–222, doi:10.1038/nature08707,
560 URL <https://www.nature.com/articles/nature08707>, number: 7278 Publisher: Nature Publishing
561 Group.
- 562 Brown, J. R., and Coauthors, 2020: Comparison of past and future simulations of ENSO in
563 CMIP5/PMIP3 and CMIP6/PMIP4 models. *Climate of the Past*, **16 (5)**, 1777–1805, doi:
564 10.5194/cp-16-1777-2020, URL <https://cp.copernicus.org/articles/16/1777/2020/>, publisher:
565 Copernicus GmbH.
- 566 Burls, N. J., L. Muir, E. M. Vincent, and A. Fedorov, 2017: Extra-tropical origin of equatorial
567 Pacific cold bias in climate models with links to cloud albedo. *Clim Dyn*, **49 (5)**, 2093–2113,
568 doi:10.1007/s00382-016-3435-6, URL <https://doi.org/10.1007/s00382-016-3435-6>.
- 569 Cai, W., and Coauthors, 2018: Increased variability of eastern Pacific El Niño under greenhouse
570 warming. *Nature*, **564 (7735)**, 201–206, doi:10.1038/s41586-018-0776-9, URL <https://www.nature.com/articles/s41586-018-0776-9>, number: 7735 Publisher: Nature Publishing Group.
- 572 Cai, W., and Coauthors, 2021: Changing El Niño–Southern Oscillation in a warming climate.
573 *Nat Rev Earth Environ*, **2 (9)**, 628–644, doi:10.1038/s43017-021-00199-z, URL <https://www.nature.com/articles/s43017-021-00199-z>, number: 9 Publisher: Nature Publishing Group.
- 575 Cane, M. A., and S. E. Zebiak, 1985: A Theory for El Niño and the Southern Oscillation. *Science*,
576 **228 (4703)**, 1085–1087, doi:10.1126/science.228.4703.1085, URL <https://science.sciencemag.org/content/228/4703/1085>, publisher: American Association for the Advancement of Science
577 Section: Reports.
- 579 Dommenges, D., T. Bayr, and C. Frauen, 2013: Analysis of the non-linearity in the pattern and
580 time evolution of El Niño southern oscillation. *Clim Dyn*, **40 (11)**, 2825–2847, doi:10.1007/
581 s00382-012-1475-0, URL <https://doi.org/10.1007/s00382-012-1475-0>.
- 582 Fang, K., and Coauthors, 2021: ENSO modulates wildfire activity in China. *Nature Communica-*
583 *tions*, **12 (1)**, 1764, doi:10.1038/s41467-021-21988-6, URL <https://www.nature.com/articles/s41467-021-21988-6>, number: 1 Publisher: Nature Publishing Group.

- 585 Fedorov, A. V., and S. G. Philander, 2000: Is El Niño Changing? *Science*, **288** (5473),
586 1997–2002, doi:10.1126/science.288.5473.1997, URL [https://science.sciencemag.org/content/](https://science.sciencemag.org/content/288/5473/1997)
587 288/5473/1997, publisher: American Association for the Advancement of Science Section:
588 Special Reviews.
- 589 Feng, R., and C. J. Poulsen, 2014: Andean elevation control on tropical Pacific climate and
590 ENSO. *Paleoceanography*, **29** (8), 795–809, doi:<https://doi.org/10.1002/2014PA002640>,
591 URL <https://agupubs.onlinelibrary.wiley.com/doi/abs/10.1002/2014PA002640>, _eprint:
592 <https://agupubs.onlinelibrary.wiley.com/doi/pdf/10.1002/2014PA002640>.
- 593 Fox-Kemper, B., S. Bachman, B. Pearson, and S. Reckinger, 2014: Principles and advances in
594 subgrid modeling for eddy-rich simulations. *CLIVAR Exchanges*, **19** (2), 42–46, URL [http://](http://bit.ly/1qSMTzA)
595 bit.ly/1qSMTzA.
- 596 Good, S. A., M. J. Martin, and N. A. Rayner, 2013: EN4: Quality controlled ocean
597 temperature and salinity profiles and monthly objective analyses with uncertainty esti-
598 mates. *Journal of Geophysical Research: Oceans*, **118** (12), 6704–6716, doi:10.1002/
599 2013JC009067, URL <https://onlinelibrary.wiley.com/doi/abs/10.1002/2013JC009067>, _eprint:
600 <https://onlinelibrary.wiley.com/doi/pdf/10.1002/2013JC009067>.
- 601 Guilyardi, E., A. Capotondi, M. Lengaigne, S. Thual, and A. T. Wittenberg, 2020:
602 ENSO Modeling. *El Niño Southern Oscillation in a Changing Climate*, Ameri-
603 can Geophysical Union (AGU), 199–226, doi:10.1002/9781119548164.ch9, URL [https://](https://agupubs.onlinelibrary.wiley.com/doi/abs/10.1002/9781119548164.ch9)
604 agupubs.onlinelibrary.wiley.com/doi/abs/10.1002/9781119548164.ch9, section: 9 _eprint:
605 <https://agupubs.onlinelibrary.wiley.com/doi/pdf/10.1002/9781119548164.ch9>.
- 606 Guilyardi, E., A. Wittenberg, A. Fedorov, C. Collins, A. Capotondi, G. J. Van Oldenborgh, and
607 T. Stockdale, 2009: Understanding El Niño in Ocean-Atmosphere General Circulation Models:
608 Progress and Challenges. *Bulletin of the American Meteorological Society*, **90**, 325–340, doi:
609 10.1175/2008BAMS2387.1.
- 610 Haine, T. W., and Coauthors, 2021: Is computational oceanography coming of age? *Bulletin of the*
611 *American Meteorological Society*, 1–33, doi:10.1175/BAMS-D-20-0258.1.

- 612 He, J., N. C. Johnson, G. A. Vecchi, B. Kirtman, A. T. Wittenberg, and S. Sturm, 2018: Precipitation
613 Sensitivity to Local Variations in Tropical Sea Surface Temperature. *Journal of Climate*, **31** (22),
614 9225–9238, doi:10.1175/JCLI-D-18-0262.1, URL [https://journals.ametsoc.org/view/journals/
615 clim/31/22/jcli-d-18-0262.1.xml](https://journals.ametsoc.org/view/journals/clim/31/22/jcli-d-18-0262.1.xml), publisher: American Meteorological Society Section: Journal
616 of Climate.
- 617 Hu, S., and A. V. Fedorov, 2018: Cross-equatorial winds control El Niño diversity and change.
618 *Nature Climate Change*, **8** (9), 798–802, doi:10.1038/s41558-018-0248-0, URL [https://www.
619 nature.com/articles/s41558-018-0248-0](https://www.nature.com/articles/s41558-018-0248-0), number: 9 Publisher: Nature Publishing Group.
- 620 Hurrell, J. W., and Coauthors, 2013: The Community Earth System Model: A Framework for
621 Collaborative Research. *Bulletin of the American Meteorological Society*, **94** (9), 1339–1360,
622 doi:10.1175/BAMS-D-12-00121.1, URL [https://journals.ametsoc.org/view/journals/bams/94/
623 9/bams-d-12-00121.1.xml](https://journals.ametsoc.org/view/journals/bams/94/9/bams-d-12-00121.1.xml), publisher: American Meteorological Society Section: Bulletin of
624 the American Meteorological Society.
- 625 Jin, F.-F., 1996: Tropical Ocean-Atmosphere Interaction, the Pacific Cold Tongue, and the El
626 Niño-Southern Oscillation. *Science*, **274** (5284), 76–78, doi:10.1126/science.274.5284.76, URL
627 <https://science.sciencemag.org/content/274/5284/76>, publisher: American Association for the
628 Advancement of Science Section: Report.
- 629 Jin, F.-F., 1997a: An Equatorial Ocean Recharge Paradigm for ENSO. Part I: Conceptual Model.
630 *Journal of the Atmospheric Sciences*, **54** (7), 811–829, doi:10.1175/1520-0469(1997)054<0811:
631 AEORPF>2.0.CO;2, URL [https://journals.ametsoc.org/view/journals/atsc/54/7/1520-0469_
632 1997_054_0811_aeorpf_2.0.co_2.xml](https://journals.ametsoc.org/view/journals/atsc/54/7/1520-0469_1997_054_0811_aeorpf_2.0.co_2.xml), publisher: American Meteorological Society Section:
633 Journal of the Atmospheric Sciences.
- 634 Jin, F.-F., 1997b: An Equatorial Ocean Recharge Paradigm for ENSO. Part II: A Stripped-
635 Down Coupled Model. *Journal of the Atmospheric Sciences*, **54** (7), 830–847, doi:
636 10.1175/1520-0469(1997)054<0830:AEORPF>2.0.CO;2, URL [https://journals.ametsoc.org/
637 view/journals/atsc/54/7/1520-0469_1997_054_0830_aeorpf_2.0.co_2.xml](https://journals.ametsoc.org/view/journals/atsc/54/7/1520-0469_1997_054_0830_aeorpf_2.0.co_2.xml), publisher: Ameri-
638 can Meteorological Society Section: Journal of the Atmospheric Sciences.
- 639 Jin, F.-F., H.-C. Chen, S. Zhao, M. Hayashi, C. Karamperidou, M. F. Stuecker, R. Xie,
640 and L. Geng, 2020: Simple ENSO Models. *El Niño Southern Oscillation in a Changing*

641 *Climate*, American Geophysical Union (AGU), 119–151, doi:10.1002/9781119548164.ch6,
642 URL <https://agupubs.onlinelibrary.wiley.com/doi/abs/10.1002/9781119548164.ch6>, section: 6
643 _eprint: <https://agupubs.onlinelibrary.wiley.com/doi/pdf/10.1002/9781119548164.ch6>.

644 Jin, F.-F., S. T. Kim, and L. Bejarano, 2006: A coupled-stability index for ENSO.
645 *Geophysical Research Letters*, **33** (23), doi:<https://doi.org/10.1029/2006GL027221>,
646 URL <https://agupubs.onlinelibrary.wiley.com/doi/abs/10.1029/2006GL027221>, _eprint:
647 <https://agupubs.onlinelibrary.wiley.com/doi/pdf/10.1029/2006GL027221>.

648 Karamperidou, C., and Coauthors, 2020: ENSO in a Changing Climate. *El*
649 *Niño Southern Oscillation in a Changing Climate*, American Geophysical
650 Union (AGU), 471–484, doi:10.1002/9781119548164.ch21, URL <https://agupubs.onlinelibrary.wiley.com/doi/abs/10.1002/9781119548164.ch21>, section: 21 _eprint:
651 <https://agupubs.onlinelibrary.wiley.com/doi/pdf/10.1002/9781119548164.ch21>.

652

653 Kim, S. T., W. Cai, F.-F. Jin, and J.-Y. Yu, 2014: ENSO stability in coupled climate models and its
654 association with mean state. *Clim Dyn*, **42** (11), 3313–3321, doi:10.1007/s00382-013-1833-6,
655 URL <https://doi.org/10.1007/s00382-013-1833-6>.

656 Kitoh, A., 2007: ENSO modulation by mountain uplift. *Clim Dyn*, **28** (7), 781–796, doi:10.1007/
657 s00382-006-0209-6, URL <https://doi.org/10.1007/s00382-006-0209-6>.

658 Kohyama, T., D. L. Hartmann, and D. S. Battisti, 2017: La Niña-like Mean-State Re-
659 sponse to Global Warming and Potential Oceanic Roles. *Journal of Climate*, **30** (11), 4207–
660 4225, doi:10.1175/JCLI-D-16-0441.1, URL [https://journals.ametsoc.org/view/journals/clim/
661 30/11/jcli-d-16-0441.1.xml](https://journals.ametsoc.org/view/journals/clim/30/11/jcli-d-16-0441.1.xml), publisher: American Meteorological Society Section: Journal of
662 Climate.

663 Lehodey, P., and Coauthors, 2020: ENSO Impact on Marine Fisheries and Ecosys-
664 tems. *El Niño Southern Oscillation in a Changing Climate*, American Geo-
665 physical Union (AGU), 429–451, doi:10.1002/9781119548164.ch19, URL [https://
666 agupubs.onlinelibrary.wiley.com/doi/abs/10.1002/9781119548164.ch19](https://agupubs.onlinelibrary.wiley.com/doi/abs/10.1002/9781119548164.ch19), section: 19 _eprint:
667 <https://agupubs.onlinelibrary.wiley.com/doi/pdf/10.1002/9781119548164.ch19>.

- 668 Levine, A., F. F. Jin, and M. J. McPhaden, 2016: Extreme Noise–Extreme El Niño: How State-
669 Dependent Noise Forcing Creates El Niño–La Niña Asymmetry. *Journal of Climate*, **29** (15),
670 5483–5499, doi:10.1175/JCLI-D-16-0091.1, URL [https://journals.ametsoc.org/view/journals/
671 clim/29/15/jcli-d-16-0091.1.xml](https://journals.ametsoc.org/view/journals/clim/29/15/jcli-d-16-0091.1.xml), publisher: American Meteorological Society Section: Journal
672 of Climate.
- 673 Lin, J.-L., 2007: The Double-ITCZ Problem in IPCC AR4 Coupled GCMs: Ocean–Atmosphere
674 Feedback Analysis. *Journal of Climate*, **20** (18), 4497–4525, doi:10.1175/JCLI4272.1,
675 URL <https://journals.ametsoc.org/view/journals/clim/20/18/jcli4272.1.xml>, publisher: Amer-
676 ican Meteorological Society Section: Journal of Climate.
- 677 McPhaden, M. J., T. Lee, S. Fournier, and M. A. Balmaseda, 2020: ENSO
678 Observations. *El Niño Southern Oscillation in a Changing Climate*, American
679 Geophysical Union (AGU), 39–63, doi:10.1002/9781119548164.ch3, URL [https://
680 agupubs.onlinelibrary.wiley.com/doi/abs/10.1002/9781119548164.ch3](https://agupubs.onlinelibrary.wiley.com/doi/abs/10.1002/9781119548164.ch3), section: 3 _eprint:
681 <https://agupubs.onlinelibrary.wiley.com/doi/pdf/10.1002/9781119548164.ch3>.
- 682 McPhaden, M. J., T. Lee, and D. McClurg, 2011: El Niño and its rela-
683 tionship to changing background conditions in the tropical Pacific Ocean.
684 *Geophysical Research Letters*, **38** (15), doi:10.1029/2011GL048275, URL
685 <https://agupubs.onlinelibrary.wiley.com/doi/abs/10.1029/2011GL048275>,
686 [_eprint:
https://agupubs.onlinelibrary.wiley.com/doi/pdf/10.1029/2011GL048275](https://agupubs.onlinelibrary.wiley.com/doi/pdf/10.1029/2011GL048275).
- 687 Naiman, Z., P. J. Goodman, J. P. Krasting, S. L. Malyshev, J. L. Russell, R. J. Stouffer, and
688 A. T. Wittenberg, 2017: Impact of Mountains on Tropical Circulation in Two Earth Sys-
689 tem Models. *Journal of Climate*, **30** (11), 4149–4163, doi:10.1175/JCLI-D-16-0512.1, URL
690 <https://journals.ametsoc.org/view/journals/clim/30/11/jcli-d-16-0512.1.xml>, publisher: Ameri-
691 can Meteorological Society Section: Journal of Climate.
- 692 Neale, R. B., J. H. Richter, and M. Jochum, 2008: The impact of convection on enso: From a
693 delayed oscillator to a series of events. *Journal of climate*, **21** (22), 5904–5924, doi:10.1175/
694 2008JCLI2244.1.
- 695 Nicholls, N., 1991: The El Niño / Southern Oscillation and Australian Vegetation. *Vegetatio*,
696 **91** (1/2), 23–36, URL <https://www.jstor.org/stable/20038710>, publisher: Springer.

- 697 Oueslati, B., and G. Bellon, 2015: The double ITCZ bias in CMIP5 models: interaction
698 between SST, large-scale circulation and precipitation. *Clim Dyn*, **44** (3), 585–607, doi:
699 10.1007/s00382-015-2468-6, URL <https://doi.org/10.1007/s00382-015-2468-6>.
- 700 Philander, S. G. H., D. Gu, G. Lambert, T. Li, D. Halpern, N.-C. Lau, and
701 R. C. Pacanowski, 1996: Why the ITCZ Is Mostly North of the Equator. *Jour-*
702 *nal of Climate*, **9** (12), 2958–2972, doi:10.1175/1520-0442(1996)009<2958:WTIIMN>2.0.
703 CO;2, URL https://journals.ametsoc.org/view/journals/clim/9/12/1520-0442_1996_009_2958_
704 [wtiimn_2_0_co_2.xml](https://journals.ametsoc.org/view/journals/clim/9/12/1520-0442_1996_009_2958_), publisher: American Meteorological Society Section: Journal of Cli-
705 mate.
- 706 Planton, Y. Y., and Coauthors, 2021: Evaluating Climate Models with the CLIVAR 2020 ENSO
707 Metrics Package. *Bulletin of the American Meteorological Society*, **102** (2), E193–E217,
708 doi:10.1175/BAMS-D-19-0337.1, URL <https://journals.ametsoc.org/view/journals/bams/102/>
709 [2/BAMS-D-19-0337.1.xml](https://journals.ametsoc.org/view/journals/bams/102/), publisher: American Meteorological Society Section: Bulletin
710 of the American Meteorological Society.
- 711 Praveen Kumar, B., J. Vialard, M. Lengaigne, V. S. N. Murty, and M. J. McPhaden, 2012: TropFlux:
712 air-sea fluxes for the global tropical oceans—description and evaluation. *Clim Dyn*, **38** (7), 1521–
713 1543, doi:10.1007/s00382-011-1115-0, URL <https://doi.org/10.1007/s00382-011-1115-0>.
- 714 Praveen Kumar, B., J. Vialard, M. Lengaigne, V. S. N. Murty, M. J. McPhaden, M. F. Cronin,
715 F. Pinsard, and K. Gopala Reddy, 2013: TropFlux wind stresses over the tropical oceans:
716 evaluation and comparison with other products. *Clim Dyn*, **40** (7), 2049–2071, doi:10.1007/
717 s00382-012-1455-4, URL <https://doi.org/10.1007/s00382-012-1455-4>.
- 718 Prieto, M. d. R., 2007: ENSO signals in South America: rains and floods in the Paraná River
719 region during colonial times. *Climatic Change*, **83** (1), 39–54, doi:10.1007/s10584-006-9188-1,
720 URL <https://doi.org/10.1007/s10584-006-9188-1>.
- 721 Rayner, N. A., D. E. Parker, E. B. Horton, C. K. Folland, L. V. Alexander, D. P.
722 Rowell, E. C. Kent, and A. Kaplan, 2003: Global analyses of sea surface tem-
723 perature, sea ice, and night marine air temperature since the late nineteenth century.
724 *Journal of Geophysical Research: Atmospheres*, **108** (D14), doi:<https://doi.org/10.1029/>

- 725 2002JD002670, URL <https://agupubs.onlinelibrary.wiley.com/doi/abs/10.1029/2002JD002670>,
726 _eprint: <https://agupubs.onlinelibrary.wiley.com/doi/pdf/10.1029/2002JD002670>.
- 727 Rodgers, K. B., P. Friederichs, and M. Latif, 2004: Tropical Pacific Decadal Variability and Its
728 Relation to Decadal Modulations of ENSO. *Journal of Climate*, **17 (19)**, 3761–3774, doi:10.
729 1175/1520-0442(2004)017<3761:TPDVAI>2.0.CO;2, URL [https://journals.ametsoc.org/view/
730 journals/clim/17/19/1520-0442_2004_017_3761_tpdvai_2.0.co_2.xml](https://journals.ametsoc.org/view/journals/clim/17/19/1520-0442_2004_017_3761_tpdvai_2.0.co_2.xml), publisher: American
731 Meteorological Society Section: Journal of Climate.
- 732 Takahashi, K., and D. S. Battisti, 2007: Processes Controlling the Mean Tropical Pacific Precip-
733 itation Pattern. Part II: The SPCZ and the Southeast Pacific Dry Zone. *Journal of Climate*,
734 **20 (23)**, 5696–5706, doi:10.1175/2007JCLI1656.1, URL [https://journals.ametsoc.org/view/
735 journals/clim/20/23/2007jcli1656.1.xml](https://journals.ametsoc.org/view/journals/clim/20/23/2007jcli1656.1.xml), publisher: American Meteorological Society Section:
736 Journal of Climate.
- 737 Wengel, C., M. Latif, W. Park, J. Harlaß, and T. Bayr, 2018: Seasonal ENSO phase locking in
738 the Kiel Climate Model: The importance of the equatorial cold sea surface temperature bias.
739 *Clim Dyn*, **50 (3)**, 901–919, doi:10.1007/s00382-017-3648-3, URL [https://doi.org/10.1007/
740 s00382-017-3648-3](https://doi.org/10.1007/s00382-017-3648-3).
- 741 Wittenberg, A. T., and Coauthors, 2018: Improved Simulations of Tropical Pacific
742 Annual-Mean Climate in the GFDL FLOR and HiFLOR Coupled GCMs. *Journal of
743 Advances in Modeling Earth Systems*, **10 (12)**, 3176–3220, doi:10.1029/2018MS001372,
744 URL <https://agupubs.onlinelibrary.wiley.com/doi/abs/10.1029/2018MS001372>,
745 [_eprint:
https://agupubs.onlinelibrary.wiley.com/doi/pdf/10.1029/2018MS001372](https://agupubs.onlinelibrary.wiley.com/doi/pdf/10.1029/2018MS001372).
- 746 Wyrtki, K., 1985: Water displacements in the Pacific and the gen-
747 esis of El Nino cycles. *Journal of Geophysical Research: Oceans*,
748 **90 (C4)**, 7129–7132, doi:<https://doi.org/10.1029/JC090iC04p07129>, URL [https://
749 //agupubs.onlinelibrary.wiley.com/doi/abs/10.1029/JC090iC04p07129](https://agupubs.onlinelibrary.wiley.com/doi/abs/10.1029/JC090iC04p07129),
750 [_eprint:
https://agupubs.onlinelibrary.wiley.com/doi/pdf/10.1029/JC090iC04p07129](https://agupubs.onlinelibrary.wiley.com/doi/pdf/10.1029/JC090iC04p07129).
- 751 Xu, W., and J.-E. Lee, 2021: The Andes and the Southeast Pacific Cold Tongue Simulation. *Journal
752 of Climate*, **34 (1)**, 415–425, doi:10.1175/JCLI-D-19-0901.1, URL <https://journals.ametsoc.org/>

753 view/journals/clim/34/1/JCLI-D-19-0901.1.xml, publisher: American Meteorological Society
754 Section: Journal of Climate.

755 Zhang, T., and D.-Z. Sun, 2014: ENSO Asymmetry in CMIP5 Models. *Journal of Climate*, **27** (11),
756 4070–4093, doi:10.1175/JCLI-D-13-00454.1, URL [https://journals.ametsoc.org/view/journals/
757 clim/27/11/jcli-d-13-00454.1.xml](https://journals.ametsoc.org/view/journals/clim/27/11/jcli-d-13-00454.1.xml), publisher: American Meteorological Society Section: Jour-
758 nal of Climate.

759 Zhao, B., and A. Fedorov, 2020: The Effects of Background Zonal and Meridional Winds on ENSO
760 in a Coupled GCM. *Journal of Climate*, **33** (6), 2075–2091, doi:10.1175/JCLI-D-18-0822.
761 1, URL <https://journals.ametsoc.org/view/journals/clim/33/6/jcli-d-18-0822.1.xml>, publisher:
762 American Meteorological Society Section: Journal of Climate.